ISSN: 2993-8643

Review Article

Engineering: Open Access

Synthesis, Spectroscopic Characterization and Application of Cu-Ni Bimetallic Hybrid Nanoparticles for the Electrochemical Sensing of Alizarin Red S

Saleem Nawaz[1], Latif ur Rahman[2]*, Syed Qaiser Shah[2], Luqman Ali Shah[3], Fatima Javed[4], Faheem Ullah[5], Noor Rehman[6], Abdullah[2] and Syed Muhammad Salman[1]

[1]*Department of Chemistry Islamia College, Peshawar, Khyber Pakhtunkhwa Pakistan*

[2]*Institute of Chemical Sciences, University of Peshawar, Khyber Pakhtunkhwa, Pakistan*

[3]*National Center of Excellence in Physical Chemistry University of Peshawar, KP Pakistan*

[4]*Department of Chemistry, Shaheed Benazir Bhutto Women University, Charsadda Road Larama, 25000, Peshawar, Pakistan*

[5]*Department of Biological Sciences, National University of Medical Sciences, (NUMS), Rawalpindi, Pakistan*

[6]*Department of Chemistry, Shaheed Benazir Bhutto University (18000) Sheringal, Dir (Upper), Khyber Pakhtunkhwa, Pakistan*

***Corresponding Author**
Latif ur Rahman, Department of Chemistry Islamia College, Peshawar, Khyber Pakhtunkhwa Pakistan.

Submitted: 2026, Sep 21; **Accepted:** 2026, Oct 30; **Published:** 2026, Nov 17

Citation: Nawaz, S., Rahman, L. U., Shah, S. O., Shah, L. A., Javed, F. U., et al. (2026). Synthesis, Spectroscopic Characterization and Application of Cu-Ni Bimetallic Hybrid Nanoparticles for the Electrochemical Sensing of Alizarin Red S. *Eng OA, 4*(11), 01-07.

Abstract

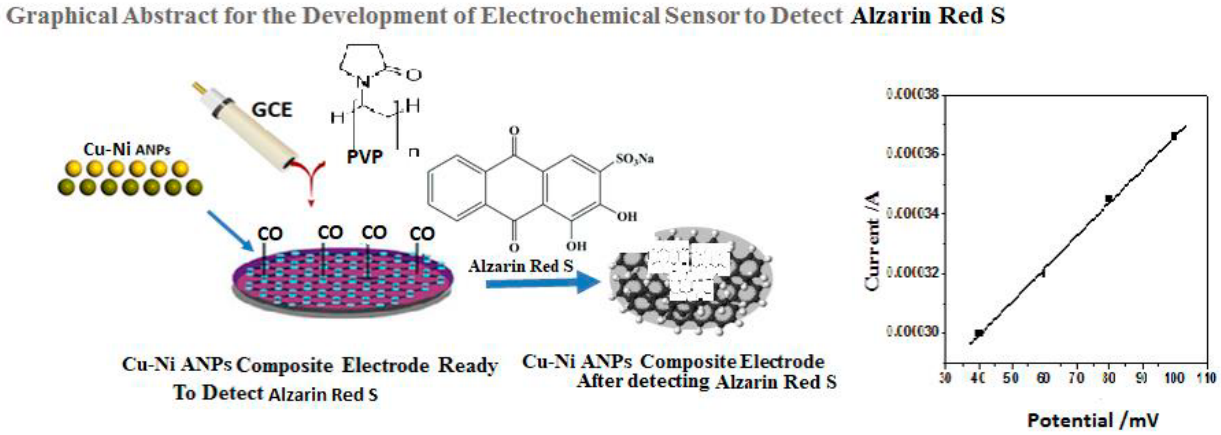
The development of a novel nanomaterial opens the windows of research in several areas. However, its optimal synthesis and characterization is a challenging task for its performance in specific fields of use. Copper-Nickle bimetallic hybrid nanoparticles (Cu-Ni-BHNPs) were manufactured by reinforcing Cu with Ni using ethylene glycol as a solvent as well as a reducing agent, and polyvinyl pyrrolidon (PVP) as a fabrication material for sensing application. UV-Vis spectroscopy, Steady-state fluorescence, Scanning Electron Microscopy (SEM), X-ray diffraction (XRD) and energy-dispersive spectroscopy (EDS) techniques were used for the confirmation and morphological studies of synthesized nanoparticles. Results display that Cu portrays enhanced characteristics in Cu-Ni-BHNPs. A composite electrode of Cu-Ni/PVP/GCE (Cu-Ni-BHNPs based electrochemical sensor) is developed by coating Cu-Ni (3:1) BHNPs embedded in PVP at the surface of cleaned Glassy Carbon Electrode (GCE). The lowest possible concentration of Alzarin Red S (0.12 µM) was detected by using Cu-Ni BHNPs based electrochemical sensor.

Highlights

- Cu-Ni bimetallic hybrid nanoparticles were chemically prepared using polyols process
- Formation of bimetallic hybrid nanoparticles was confirmed by UV-Visible spectroscopy and their size was determined by x-ray diffraction spectroscopy (XRD) and scanning electron microscopy (SEM)

- Composite electrode (Cu-Ni3:1NPs/PVP/GCE) was developed by drop coating of NPs on cleaned glassy carbon electrode (GCE)
- Sensitivity of the composite electrode for the detection of Alzarin Red S was checked out by square wave voltammetry (SWV), electrochemical impedance spectroscopy (EIS) and cyclic voltammetry (CV)
- Alzarin Red S at the composite electrode exhibits a higher electro catalytic effect than bare GCE.

Graphical Abstracts



Keywords: Cu-Ni Bimetallic Hybrid Nanoparticles (BHNPs), Poly Vinyl Pyrrolidon (PVP), Ethylene Glycol, Electrochemical Sensor, Alzarin Red S

1. Introduction

There are plenty of uses of nanoparticles (NPs) in various domains of life. Whether they are monometallic or bimetallic, NPs exhibit useful characteristics that support our work in a variety of scientific domains. Their form and size are ascribed to these distinctive characteristics [1]. Because of their distinct physicochemical characteristics in comparison to monometallic nanoparticles, bimetallic nanoparticles (BNPs) have garnered the interest of scientists and technologists in recent years [2]. The characteristics of BNPs are dependent on their size, content, and shape [3]. By detecting other species in their surroundings, bimetallic alloy nanoparticles' (BANPs) surface physiochemical characteristics can vary, which can aid in the detection of hazardous and carcinogenic chemicals such as polycyclic aromatic hydrocarbons (PAHs). To monitor one of the dangerous and environmentally poisons PAHs, bimetallic hybrid nanoparticles (BHNPs) may be utilized [4]. Cu and Ni BANPs' unique surface has been functionalized, which has been used in electronics/electro-optical devices, biosensing, catalysis, and electronics/electro-optical devices [5-7]. Cu and Ni NPs and their nanoalloys are employed as sensors because of their distinctive characteristics [8-12].

Many BNPs have been thoroughly investigated for their potential as electrochemical sensors. However, there has been little research done on Cu-Ni-BHNPs based electrochemical sensing applications. Additionally, Cu and Ni NPs are less expensive than other pricey metals like gold, platinum, etc., they provide excellent candidates for the fabrication of electrochemical sensors [13-14]. According to one publication, exposure to an open environment poses a significant obstacle to the use of Cu NPs in the manufacture of sensors. By suggesting Cu and Ni BHNPs that regulate the decomposing action, this problem was resolved [15].

Using chemical reduction methods, a variety of electrochemical sensors based on Cu-Ni-BHNPs are meticulously constructed in the current research work. Ultimately, cyclic voltammetry (CV) and electrochemical impedance spectroscopy (EIS) methods were used to examine the electrochemical sensing properties of the different test samples of BHNPs. Cu-Ni (3:1) BHNPs has demonstrated the highest sensing performance among all test samples when it comes to the detection of the worst environmental pollutants and carcinogenic dye Alizarin Red S (ARS).

2. Experimental

2.1. Method and Materials

All the compounds used to conduct the present research work were of research standard and did not require any additional purification. Different chemicals used during study included Nickle nitrate hexahydrate (NiNO3.6H2O), Copper (II) nitrate trihydrate (Cu(NO3)2.3H2O), Polyvinylpyrrolidone (PVP) MW = 10,000g and ethylene glycol. All glass wares were washed beforehand with HCl solution and then repeatedly rinsed with distilled water.

2.2. Cu and Ni Nanoparticles Synthesis

To prepare 10 mM copper ions solution, 30 mL of ethylene glycol was mixed with the necessary amount of $Cu(NO_3)_2.3H_2O$. A 10 mM PVP solution was prepared in another flask by dissolving a precisely estimated quantity of PVP-10,000 in 30 mL of ethylene glycol and stirring the mixture for 10 minutes. 10 mL of $Cu(NO_3)_2.3H_2O$ (10 mM) and 10 mL of PVP (10 mM) were combined for the production of Cu nanoparticles while being continuously stirred and heated to 150 °C for 15 minutes.

To prepare 10 mM nickle ions solution, 30 mL of ethylene glycol was mixed with the necessary amount of $NiNO_3.6H_2O$. 10 mL of $NiNO_3.6H_2O$ (10 mM) and 10 mL of PVP (1 mM) were combined for the production of Ni nanoparticles while being continuously stirred and heated to 170 °C for 20 minutes.

2.3. Cu-Ni Hybrid Bimetallic Nanoparticles (HBNPs) Synthesis

5 mL of $Cu(NO_3)2.3H2O$ solution (10 mM) was mixed with 5 mL of NiNO3.6H2O solution (10 mM) and 5 mL of PVP (10 mM) to create Cu-Ni bimetallic hybrid nanoparticles (BHNPs). The colloidal mixture was heated at 175 oC for thirty minutes with constant stirring.

3. Results and Discussions

3.1. UV/ Visible Spectroscopy

Since Ni and Cu NPs have been reported to produce surface plasmon response (SPR) bands within that particular range, a UV-visible spectrum was obtained between 350 and 800 nm [16]. These surface charge oscillations are quantized and are caused by an external electric field. Fascinating optical characteristics are produced by SPR stimulated metal nanoparticles. With UV-Vis Spectroscopy, these resonances may be examined in bulk solution [17]. The size, shape, and kind of particles, together with the solvent used in the synthesis, all have an impact on the SPR peaks; the wider the bandwidth of an SPR band, the smaller the nanoparticle size [18].

The UV/visible spectrum of Cu NPs' is depicted in Figure 1A with the highest absorption peak at 580 nm, which is quite similar to the value of 575 nm reported in the literature [19]. The UV/visible spectrum of Ni NPs, with a maximum absorption at 275 nm, is displayed in Figure 1B. According to the observed data, there is a larger absorbance peak at around 275 nm, and the distinctive peak of SPR appears in the spectrum at 365 nm as a little shoulder, revealing that the nickel salt solution has been converted to Ni NPs [20].

The UV-visible spectra of Cu-Ni BHNPs created in different ratios, such as 1:1, 2:1, and 3:1, exhibit a red shift as the content of Cu increases. Cu-Ni BHNPs have been generated as shown by Figure 1C, as proven by the existence of a single UV/visible absorbance peak at these wave lengths, which are between 275 nm (for pure nickel) and 575 nm (for pure copper). This demonstrates that the produced NPs were hybrid nanoparticles rather than mixtures of elemental NPs [19-21].

Figure 2a shows the UV/visible spectrum of 1:1 Cu-Ni-BHNPs having maximum absorbance at 431 nm and the absorbance vs concentration plot of Cu-Ni (1:1) BHNPs which gives a straight line with slope giving molar absorptivity equal to 77.26 liters/mole.cm this shows the data is following beer lambert law as shown by Equation 1.

$$A = \in Cl \quad 1$$

Figure 2b shows the UV/visible spectrum of 1:2 Cu-Ni BHNPs having maximum absorbance at 450 nm. The absorbance value got decreased as the colloidal solution is diluted and get vanished at 0.05 concentrations. Figure 2b also shows the absorbance vs concentration plot of Cu-Ni (1:2) BHNPs which gives a straight line with slope giving molar absorptivity equal to 54.6 liters/mole.cm hence the data is obeying beer lambert law. Figure 2c shows the UV/visible spectrum of Cu-Ni 3:1 BHNPs having maximum absorbance at 500 nm. The Figure 2C also reflects the beer lambert law plot of Cu-Ni (1:3) BHNPs which gives a straight line with slope giving molar absorptivity equal to 94.5 liters/mole.cm. The result obtained from UV/visible spectroscopic analysis of mono and BHNPs of Cu and Ni combined in 1:1, 1:2 and 3:1 mole ratio are depicted in Table 1. As clear from Table 1 the value of molar absorptivity is highest for Cu-Ni ratio 3:1. So Cu-Ni BHNPs are selected for farther analysis.

3.2. Fluorescence Spectra of Cu-Ni-BHNPs

Figure 3a graphically explain fluorescence emission spectra of Cu-Ni-BHNPs at varying mole fraction of Cu. Copper and nickel nanoparticles in a physically mixed solution exhibit two different emission spectra, while the BHNPs have a single emission peak, confirming the synthetic process. The maximum intensity peaks appear at 612 to 617 with a slight red and decline in fluorescence intensity with rise in the mole fraction of Cu in the Cu-Ni BHNPs samples, thus Cu acts as quencher.

The concentration of the sample and quencher influences the intensity both in the presence and absence of the quencher.

$$ln\frac{I_o}{I_Q} = \frac{[Q]N}{[X]} \qquad 2$$

Where in Equation 2 quencher concentration is represented by [Q], while sample molar concentration by [X]. N is the estimated number of atoms in the nanoparticle. Io and IQ express the emission intensity in the absence and presence of quencher. Plotting $logI_o/IQ$ versus [Q]/[X] is shown in Figure 3b. The value of N is 491 calculated from the slope. At low concentration the quenching of fluorescence in solution follow classical Stern-Volmer equation [22].

$$(I_o - I_Q)/I_Q = K_{sv}[Q] \qquad 3$$

Where in Equation 3, K_{sv} is Stern-Volmer constant or quenching constant. The slope of $(I_o$-IQ)/IQ versus [Q] yield the quenching constant, which is computed and displayed in Figure 3c. The value of quenching constant or Stern-Volmer constant obtained from plot is 210 M^{-1}.

To find binding constant, binding energy and approximate number of binding sites logarithmic form of modified Stern-Volmer equation is used given below [23].

$$\frac{\log(I_o - I_Q)}{I_Q} = \log K_b + \text{nlog}[Q] \qquad 4$$

In Equation 4, n represent the total amount of binding sites estimated by the slope of $\frac{\log(I_o - I_Q)}{I_Q}$ vs $\log[Q]$, Kb is binding constant obtained from intercept of the curve. Binding energy ΔG_b is calculated from K_b using following Equation 5.

$$\Delta G_b = -RTlnK_b \qquad 5$$

Figure 3d shows plot of modified Stern-Volmer. The value of obtained from plot is 1.67 while k_b calculated from intercept is 184.93 while binding energy calculated from intercept is 12.93 kJ/mole.

3.3. Characterizations of Cu-Ni-BHNPs

Figure 4 shows SEM images of Cu-Ni-BHNPs having 1:1, 2:1 and 3: 1 mole ratio. The average particle sizes calculated from SEM images are 35nm for Cu-Ni (3:1) 64nm for Cu-Ni (2:1) and 95nm for Cu-Ni (1:1). It is clear from images that Cu-Ni (3:1) show smaller and more uniform particle size [24].

Figure 5 shows EDX spectra of Cu-Ni-BHNPs having 1:1, 2:1 and 3:1 composition. The existence of Ni and Cu peaks in the EDX results and lack of any other distinctive peaks indicates their presence in NPs. Therefore, these results provide strong proof that the Cu-Ni BHNPs are pure and devoid of any additional constituents [25]. As we increase the mole ratio of Cu in nanoparticles the Cu peak in spectra enhances while the Ni peaks show a corresponding decrease. Hence the outcomes of EDX analysis correspond with the mole ratios of Cu^{2+} to Ni^{2+} used in the creation of nanoparticles.

The X-ray diffraction pattern was utilized to diagnose the structural phases of Cu-Ni-BHNPs. Figure 6 displays the XRD patterns of the 1:1, 2:1 and 3:1 compositions synthetic Ni-Cu BHNPs. Plot of x-rays' intensity vs 2θ give sharp peaks which confirms the crystalline nature of NPs. Sharp and intense diffraction peaks at 2θ appeared at 40.9°, 49.9°, and 75.85º, corresponding to the (111), (200), and (220) planes. These peaks suggested the creation of pure cubic Cu−Ni BHNPs. An advancing (red) shift of the Bragg peaks to lesser diffraction angles takes place as the Ni content decreases which are in accordance with result reported in literature [24,25]. Scherrer's formula was used to compute the average crystallite size, from the diffraction peaks was found to be 35−49 nm for Ni−Cu-BHNPs and particle size decreases as Cu composition is increase [26,27].

3.4. Electrochemical Applications of Cu-Ni-BHNPs

The cyclic voltammetry (CV) studies indicated that dye shows irreversible cyclic voltammetric behaviour of Cu-Ni BHNPs having compositions 1:1, 2:1 and 3:1 as displayed in Figure 7 shows cyclic voltamograms of bare GCE electrode, Polyvinyl pyrrolidon (PVP) modified GCE electrode, Cu-Ni (1:1, 2:1 and 3;1) BHNPs modified GCE electrode and Cu-Ni(3:1)-PVP modified GCE electrode showing well-defined peaks at 0.29 mV for BHNPs modified electrodes as shown in Table 3. The PVP-Cu-Ni framework makes the electron transfer easier of dyes, which substantially boosts the current [28]. Hence, it is clear from the value of Ip obtained which is highest for PVP-Cu-Ni BHNPs modified electrode (0.08 mA) hence giving best sensitivity for detection of Alizarin red S as compare to

bare GCE and Cu-Ni BHNPs modified GCE electrode.

SWV was used to examine the PVP-Cu-Ni (3:1) /GCE performance under idealized circumstances. Figure 8a displays the recorded voltammograms with ARS concentrations ranging from 10 μM to 1μM. In accordance with IUPAC recommendations, the developed sensor's ARS limit of detection (LOD) was determined [29]. The blank solution's peak current data were used to compute the standard deviation for PVP-Cu-Ni(3:1)/GCE. PVP-Cu-Ni(3:1)/GCE is a promising method for microscopic level tracing of selected dye, as evidenced by the limit of detection (LOD) value of ARS of 0.12 μM.

Experiments on the reproducibility and repeatability of the developed sensor verified its validity. As seen in Figure 8a, voltammograms were obtained under ideal circumstances after four electrodes were similarly changed for this purpose. Similar peak current readings on the ARS show that the proposed electrochemical sensor has high repeatability, with an RSD of less than 5%. As seen in Figure 8b, a repeatability experiment including several measurements on the same electrode at various time intervals revealed that the PVP-Cu-Ni/GCE was stable, with an RSD < 5%.

Electrochemical impedance spectroscopy, (EIS) provides important details on the characteristics of charge transport at the sensor surface. In a 5 mM $K_3[F_e(CN)_6]$ redox probe in 0.1 M KCl electrolyte, the EIS measurement of GCE and Cu-Ni-BHNPs modified GCE was performed at 14 kHz to 1 Hz frequency range. The bare and modified GCE's Nyquist charts are displayed in Figure 9. However, PVP modified GCE shows smaller semicircle than bare GCE due to electron transfer facilitation offered by conducting polymer PVP. The largest semicircle diameter of bare GCE compared to Cu-Ni/GCE exhibit a rapid charge transfer process at modified electrode vis-a-vis bare electrode. The smallest semicircle is evidenced by GCE modified by PVP as well as Cu-Ni (3:1) BHNPs called composite electrode of electrochemical sensor indicates that Cu-Ni BHNPs further improve the electron transfer mechanism and retards the resistance to electrons, and thence the target dye (ARS was easily sensed with its lowest concentration in aqueous media).

The R_{ct} values obtained for PVP-Cu-Ni/GCE ((2.18 kΩ) is lowest than that for bare GCE (8.51 kΩ) and GCE modified with PVP (8.1 kΩ) and Cu-Ni (3:1) BHNPs (4.75 kΩ) alone. Due to a larger electroactive surface area, the developed electrochemical sensor's optimal charge transport is shown by a reduced Rct value for Cu-Ni/GCE [29]. The modifier serves as a conduit between the sensor and the substance being tested, giving the bare GCE improved electrical characteristics [30]. Rct and other EIS parameters were computed using the Randles equivalent circuit, which is depicted in Table 4. Using Randles-Sevic equation the active surface area of bare GCE, Cu-Ni (3:1)/GCE and PVP/Cu-Ni (3:1)/GCE were calculated. The surface area values calculated for Cu-Ni/GCE and PVP-Cu-Ni/GCE was 5.1 and 5.8 times greater than surface area of bare GCE. The information resulted from EIS strongly supports the results of CV and SWV giving a back to use PVP-Cu-Ni (3:1)/GCE as a sensing platform of sensing of ARS.

4. Conclusion

Cu-Ni-BHNPs were synthesized via polyol method. Spectroscopic study of nanoparticles shows that the wave length of maximum absorbance for Cu-Ni BHNPs is between the wave length maxima of Cu and Ni monometallic NPs with red shift due to increase in Cu mole ratio. Fluorescence spectra of Cu-Ni-BHNPs shows that Cu act as quencher and emission intensity decreases with increase in Cu mole ratio. An environmental friendly method was developed for the detection of Alizarin red S (ARS) using Cu-Ni-BHNPs. PVP was used as capping as well as electrochemical sensing facilitator. The electrochemical catalytic behavior of Cu-Ni-BHNPs was found to depend on the Cu:Ni molar ratio. Cu-Ni (3:1) BHNPs exhibited higher Ip and lower Rct value than the other Cu-Ni BHNPs which make it the best choice. It is concluded that the designed electrochemical sensor (Cu-Ni (3:1) BHNPs/GCE) is the most successful detector for ARS in industrial waste water with LOD value of 0.12μM.

Acknowledgments

This work was jointly supported by Institute of Chemical Sciences University of Peshawar and National Center of Excellence in Physical Chemistry University of Peshawar. The financial support of Higher Education Commission of Pakistan and Islamia College Peshawar is also acknowledged.

CRediT Authorship Contribution Statement

- **Saleem Nawaz:** Conceptualization, Methodology, Investigation, Software, Data curation, Writing – original draft.
- **Latif ur Rahman:** Supervision, Software, Validation, Writing – review & editing.
- **Syed Qaiser Shah:** Conceptualization, Methodology, Investigation, Software, Data curation.
- **Luqman Ali Shah:** Visualization and reviewing.
- **Fatima Javed:** Conceptualization Software, Validation, Writing – review & editing.
- **Faheem Ullah:** Software, Validation, Writing – review & editing.
- **Noor Rehman:** Visualization and software.
- **Abdullah:** Software, Validation, Conceptualization, Writing – review & editing.

- **Syed Muhammad Salman:** Visualization, Validation, software.

Declaration of Competing Interest

It is stated that the manuscript entitled Synthesis, spectroscopic characterization and application of Cu-Ni bimetallic hybrid nanoparticles for the electrochemical sensing of Alizarin Red S is a novel research. The authors declare no competing financial interest. The coauthors have contributed equally and their contributions has been highlighted by writing their names at the start. All the authors have been informed during writing and submission of this article.

Data Availability

No data was used for the research described in the article.

References

1. Shah, A., Han, C., & Jan, A. K. (2020). Monitoring of anthracene using nanoscale Au–Cu bimetallic alloy nanoparticles synthesized with various compositions. *ACS omega, 5*(35), 22494.
2. Sharma, G., Gupta, V. K., Agarwal, S., Kumar, A., Thakur, S., & Pathania, D. (2016). Fabrication and characterization of Fe@ MoPO nanoparticles: ion exchange behavior and photocatalytic activity against malachite green. *Journal of Molecular Liquids, 219*, 1137-1143.
3. Shah, A., Qureshi, R., Khan, S. B., Asiri, A. M., Shah, A. U. H. A., Ishaq, M., ... & Zia, M. A. (2015). Spectroscopic analysis of Au-Cu alloy nanoparticles of various compositions synthesized by a chemical reduction method. *Advances in Materials Science and Engineering, 2015*(1), 638629.
4. Shah, A., Khan, S. B., Asiri, A. M., Hussain, H., Han, C., Qureshi, R., ... & Kraatz, H. B. (2015). Synthesis, characterization, and application of Au–Ag alloy nanoparticles for the sensing of an environmental toxin, pyrene. *Journal of Applied Electrochemistry, 45*(5), 463-472.
5. Zhang, S., Geryak, R., Geldmeier, J., Kim, S., & Tsukruk, V. V. (2017). Synthesis, assembly, and applications of hybrid nanostructures for biosensing. *Chemical reviews, 117*(20), 12942-13038.
6. Menazea, A. A., & Ahmed, M. K. (2020). Silver and copper oxide nanoparticles-decorated graphene oxide via pulsed laser ablation technique: Preparation, characterization, and photoactivated antibacterial activity. *Nano-Structures & Nano-Objects, 22*, 100464.
7. Menazea, A. A., & Ahmed, M. K. (2020). Synthesis and antibacterial activity of graphene oxide decorated by silver and copper oxide nanoparticles. *Journal of Molecular Structure, 1218,* 128536.
8. Varagnolo, S., Lee, J., Amari, H., & Hatton, R. A. (2020). Selective deposition of silver and copper films by condensation coefficient modulation. *Materials Horizons, 7*(1), 143-148.
9. Ali, A., Baheti, V., Vik, M., & Militky, J. (2020). Copper electroless plating of cotton fabrics after surface activation with deposition of silver and copper nanoparticles. *Journal of Physics and Chemistry of Solids, 137,* 109181.
10. Huang, C., Chen, X., Xue, Z., & Wang, T. (2020). Effect of structure: A new insight into nanoparticle assemblies from inanimate to animate. *Science advances, 6*(20), eaba1321.
11. Khalilzadeh, M. A., Tajik, S., Beitollahi, H., & Venditti, R. A. (2020). Green synthesis of magnetic nanocomposite with iron oxide deposited on cellulose nanocrystals with copper (Fe3O4@ CNC/Cu): investigation of catalytic activity for the development of a venlafaxine electrochemical sensor. *Industrial & Engineering Chemistry Research, 59*(10), 4219-4228.
12. Rahman, L. U., Shah, A., Lunsford, S. K., Han, C., Nadagouda, M. N., Sahle-Demessie, E., ... & Dionysiou, D. D. (2015). Monitoring of 2-butanone using a Ag–Cu bimetallic alloy nanoscale electrochemical sensor. *RSC advances, 5*(55), 44427-44434.
13. Liu, W. W., Jiang, W., Liu, Y. C., Niu, W. J., Liu, M. C., Zhao, K., ... & Chueh, Y. L. (2020). Platinum-free ternary metallic selenides as nanostructured counter electrode for high-efficiency dye-sensitized solar cell by interface engineering. *ACS Applied Energy Materials, 3*(4), 3704-3713.
14. Khan, N. A., Rashid, N., Junaid, M., Zafar, M. N., Faheem, M., & Ahmad, I. (2019). NiO/NiS heterostructures: an efficient and stable electrocatalyst for oxygen evolution reaction. *ACS Applied Energy Materials, 2*(5), 3587-3594.
15. Shafa, M., Ahmad, I., Hussain, S., Asif, M., Pan, Y., Zairov, R., ... & Jabeen, U. (2023). Ag-Cu nanoalloys: An electrochemical sensor for H2O2 detection. *Surfaces and Interfaces, 36,* 102616.
16. Tsuji, M., Hikino, S., Tanabe, R., Matsunaga, M., & Sano, Y. (2010). Syntheses of Ag/Cu alloy and Ag/Cu alloy core Cu shell nanoparticles using a polyol method. *CrystEngComm, 12*(11), 3900-3908.
17. Shibata, T., Bunker, B. A., Zhang, Z., Meisel, D., Vardeman, C. F., & Gezelter, J. D. (2002). Size-dependent spontaneous alloying of Au− Ag nanoparticles. *Journal of the American Chemical Society, 124*(40), 11989-11996.
18. Quevedo, A. C., Guggenheim, E., Briffa, S. M., Adams, J., Lofts, S., Kwak, M., ... & Valsami-Jones, E. (2021). UV-Vis spectroscopic characterization of nanomaterials in aqueous media. JoVE (Journal of Visualized Experiments), (176), e61764.
19. Ramyadevi, J., Jeyasubramanian, K., Marikani, A., Rajakumar, G., Rahuman, A. A., Santhoshkumar, T., ... & Marimuthu, S. (2011). Copper nanoparticles synthesized by polyol process used to control hematophagous parasites. *Parasitology research, 109*(5), 1403-1415.

20. S. Sreenivasagan, A.K. Subramanian, S. Rajeshkumar Uv-Vis spectroscopy of silver nanoparticles and toxicology evaluation of silver nanoparticle based oral rinse on embryonic development of zebrafish, J. Complement. Med. *Res. 12* (2021) 85-85.
21. Pal, A., Shah, S., Kulkarni, V., Murthy, R. S. R., & Devi, S. (2009). Template free synthesis of silver–gold alloy nanoparticles and cellular uptake of gold nanoparticles in Chinese Hamster Ovary cell. *Materials Chemistry and Physics, 113*(1), 276-282.
22. Keizer, J. (1983). Nonlinear fluorescence quenching and the origin of positive curvature in Stern-Volmer plots. *Journal of the American Chemical Society, 105*(6), 1494-1498.
23. https://link.springer.com/article/10.1007/s10895-010-0657-6https://link.springer.com/article/10.1007/s10895-010-0657-6.
24. Mary, J. A., Manikandan, A., Kennedy, L. J., Bououdina, M., Sundaram, R., & Vijaya, J. J. (2014). Structure and magnetic properties of Cu-Ni alloy nanoparticles prepared by rapid microwave combustion method. *Transactions of Nonferrous Metals Society of China, 24*(5), 1467-1473.
25. Beković, M., Ban, I., Drofenik, M., & Stergar, J. (2023). Magnetic nanoparticles as mediators for magnetic hyperthermia therapy applications: a status review. *Applied Sciences, 13*(17), 9548.
26. He, K., Chen, N., Wang, C., Wei, L., & Chen, J. (2018). Method for determining crystal grain size by x-ray diffraction. *Crystal Research and Technology, 53*(2), 1700157.
27. Al Husaeni, D. F. (2021). How to Calculate Crystallite Size from X-Ray Diffraction (XRD) using Scherrer Method. *ASEAN Journal of Science and Engineering.*
28. Lipskikh, O. I., Korotkova, E. I., Barek, J., Vyskocil, V., Saqib, M., & Khristunova, E. P. (2020). Simultaneous voltammetric determination of Brilliant Blue FCF and Tartrazine for food quality control. *Talanta, 218,* 121136.
29. Rajawat, D. S., Srivastava, S., & Satsangee, S. P. (2012). Electrochemical determination of mercury at trace levels using eichhornia crassipes modified carbon paste electrode. *International Journal of Electrochemical Science, 7*(11), 11456-11469.
30. Sierra-Rosales, P., Toledo-Neira, C., & Squella, J. A. (2017). Electrochemical determination of food colorants in soft drinks using MWCNT-modified GCEs. *Sensors and Actuators B: Chemical, 240,* 1257-1264.

Copyright: *©2026 Latif ur Rahman, et al. This is an open-access article distributed under the terms of the Creative Commons Attribution License, which permits unrestricted use, distribution, and reproduction in any medium, provided the original author and source are credited.*